

MULTI-LEVEL EXPLANATIONS IN NEUROSCIENCE II: EEG SPECTRAL FINGERPRINTS AND TENSOR DECOMPOSITIONS FOR UNDERSTANDING BRAIN ACTIVITY — INITIAL RESULTS*

MICHAŁ K. KOMOROWSKI^{a,b}, MANSOUREH AGHABEIG^{a,b}
JAN NIKADON^{a,b}, TOMASZ PIOTROWSKI^{a,b}, JOANNA DRESZER^{a,c}
BIBIANNA BALAJ^{a,c}, MONIKA LEWANDOWSKA^{a,c}
JAKUB WOJCIECHOWSKI^d, NATALIA PAWLACZYK^a
MAGDALENA SZMYTKA^a, ANDRZEJ CICHOCKI^b, WŁODZISŁAW DUCH^{a,b,†}

^aNeurocognitive Laboratory, Center for Modern Interdisciplinary Technologies
Nicolaus Copernicus University, Toruń, Poland

^bDepartment of Informatics, Faculty of Physics, Astronomy and Informatics
Nicolaus Copernicus University, Toruń, Poland

^cDepartment of Psychology, Faculty of Humanities
Nicolaus Copernicus University, Toruń, Poland

^dNencki Institute of Experimental Biology of Polish Academy of Science
Neurophysiology Department, Warszawa, Poland

(Received November 6, 2018)

Two examples of multi-level explanations of brain activity are provided. First study is aimed at extraction of information from EEG to recognize which brain regions are active using spectral fingerprinting. It is based on forward and inverse modeling of electric potentials measured by sensors placed on the scalp, and computing power spectra from different brain locations. Reliable recognition of specific brain activity using EEG may lead to better diagnostic and therapeutic methods, and various new ways of building brain-computer interfaces. In the second study, infant EEG data collected at our BabyLAB were used to derive Event-Related Potentials (ERPs), in an oddball paradigm with two types of deviant stimuli (easy and hard) and one standard stimuli. Tensor decomposition of these signals, conforming to non-negative Canonical Polyadic decomposition (NCPD) model and non-negative Tucker decomposition (NTD), is used to characterize differences in processing these stimuli. Multi-domain temporal, spectral, time-frequency representation (TFR) and spatial information features are simultaneously analyzed for more reliable representation of the underlying

* Presented at the LVIII Cracow School of Theoretical Physics “Neuroscience: Machine Learning Meets Fundamental Theory”, Zakopane, Poland, June 15–23, 2018.

† Corresponding author: wduch@is.umk.pl

source of brain activity. Results show right-side asymmetry for 5-frequency (Hz) theta band and may be due to the dynamical process of expectancy and surprise, corresponding to deviant detection reflected in the mismatch response.

DOI:10.5506/APhysPolB.49.2011

1. Introduction

Mapping brain dynamics into mental states to understand behavior [1] and describing social interactions between people [2] is a great challenge for physics of complex systems. During resting state, when people are not performing any specific tasks, different quasi-stable networks can be extracted from the functional Magnetic Resonance (fMRI) recordings of the human brain signals [3]. Moreover, different brain regions have natural frequencies of oscillations coupling cortex and thalamus structures (corticothalamic loops). This has been shown by perturbing selected corticothalamic loops using transcranial magnetic stimulation (TMS) and analyzing high-density electroencephalograms to measure their natural frequency [4]. Such functional coupling patterns across distributed brain regions have stable core features for various task states, ranging from simple passive fixation to complex classification tasks [5]. These large-scale networks may also be activated during longer resting-state activity, reflecting the functional architecture of cortical networks [6] and thus can serve as a starting point for the analysis of general brain function.

One way to see fingerprints of individual brain areas activity, developed recently by Keitel and Gross [7], is based on the local power spectra. Spectral fingerprints were obtained from magnetoencephalographic (MEG) recordings in the resting state. MEG has some advantages over the EEG, recording oscillations up to 120 Hz (called high gamma), while EEG rarely goes over 60 Hz due to the noise and low amplitude of high-frequency signals. Both EEG/MEG sensors receive linear superposition of contributions from many brain areas. Source reconstruction requires first forward propagation models and then solution of ill-posed inverse problem for source localization [8].

Previous studies of localized power spectra [9, 10] were not comprehensive, focusing only on particular frequency band, or only on particular brain areas. Keitel and Gross paper [7] includes broadband analysis of all regions of cortex, taking into account transitions between different large scale functional networks changing frequency spectrum over time. Their approach allowed for comprehensive characterization of intrinsic spectral activity of many anatomical areas during resting state. However, MEG is an expensive technique and it is of great theoretical and practical interest to perform similar study using high-density EEG recordings.

2. Spectral fingerprinting procedure

Computing spectral fingerprints starts with multivariate MEG signal (cleaned from artifacts [11, 12]) and individual structural scans or head models [13, 14] for a group of subjects. The output consists of multiple spectral profiles assigned to each of the studied brain regions (Fig. 1). Each power spectrum (called ‘profile’ or ‘cluster’) represents a different mode of brain activity that can be generalized across participants. To calculate it, following steps need to be performed:

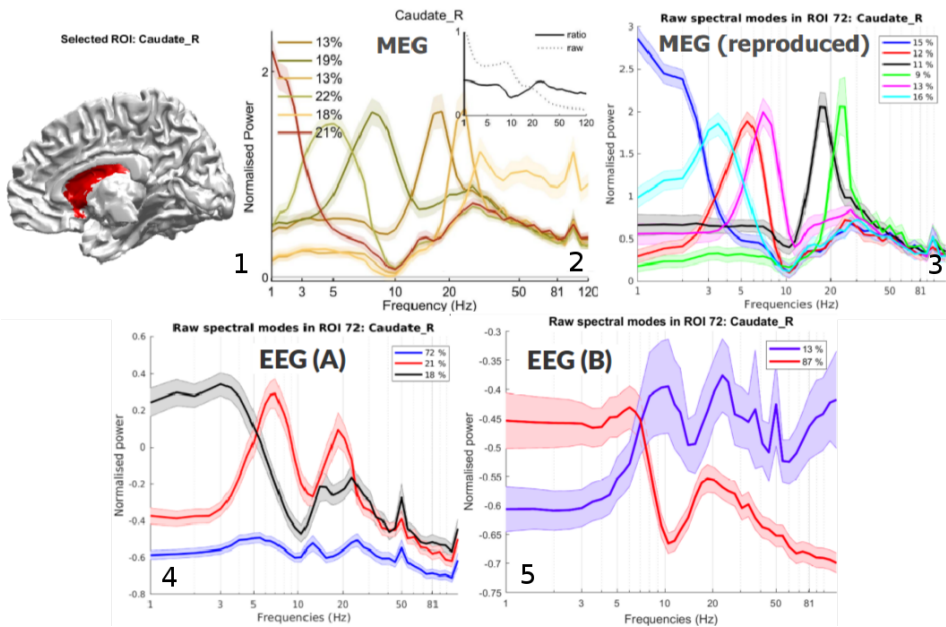


Fig. 1. Spectral fingerprint of the caudate nucleus. Pictures from left: (1) Caudate nucleus (right part) highlighted according to its coordinates from AAL [15] brain atlas. (2) Clustered power spectra of the caudate nucleus (normalized power, *i.e.*, spectral power in comparison to the whole brain). Legend shows the corresponding duration of each pattern (*i.e.*, the percentage of time segments in which each spectrum was present on average during whole recording). Shaded error bars illustrate the standard error of the mean across participants. Inlets show average power spectra for respective areas without normalization (dotted lines) and with ratio normalization (continuous lines) [7]. (3) Analogous spectral fingerprint was obtained from our replication on the same MEG data, (4) using EEG data from the Age-ility Project [16], and (5) using EEG data recorded in our laboratory.

1. Selection of the signal data from the time interval of interest and division to subsequent short-time windows (*e.g.* 1 second segments).
2. Estimation of frequency spectrum for each time segment [17, 18].
3. Computation of the forward model of the human brain to describe how source activity is propagated to sensors based on conductivity of different types of brain tissue [14].
4. Solve the inverse problem to estimate frequency spectrum of the particular brain region (Region Of Interest, ROI) by utilizing source analysis methods [14, 19–21].
5. Calculation of spectral profiles for each individual subject [7] for each ROI. Each profile potentially represents involvement of that ROI in different functional brain network state.
6. For each ROI: clustering centers of profiles from all participants, and clustering these again to obtain spectral profiles representing brain dynamics states generalizable across participants. Each profile could be viewed as a particular mode of brain activity and it is plotted as the spectrum with a dominant peak/valley. A set of profiles belonging to each ROI is called Spectral Fingerprint (SF) of that ROI (see Fig. 1).

3. Spectral Fingerprinting

3.1. Remarks on the MEG signal

The method is able to untangle spectral modes of brain areas and allowed for the extraction of invariant SFs that generalize across participants, as it was shown in [7]. Following conclusions were stated:

- individual brain areas can be identified from spectral profiles with high accuracy,
- clustering of brain areas according to the similarity of spectral profiles reveals well-known brain networks,
- activity modulation is visible as a shift of spectral modes.

Original MEG dataset (MEG-O) consisted of data from 22 subjects recorded in resting-state condition, with analyzed signal length of 466 ± 20 s. This dataset, obtained from the authors, have been used in our attempt to reproduce the results from the original article [7]. We have also used a subset of this data, labeled MEG-R, that was open to the public. The spectral

fingerprinting procedure can also be used with some adjustments to study oscillations from EEG recordings. We have re-implemented the method and used it on two separate EEG datasets recorded in the resting-state conditions. First EEG dataset (EEG-A) was obtained from the Age-ility Project that provided open data [16]. Subjects were asked to sit and rest with their eyes closed. The length of the signal was 118 ± 7 s for each of the 22 subjects participating in this study. Second EEG dataset (EEG-B) was collected in our laboratory and included $N = 12$ subjects recorded in exactly the same conditions as the MEG dataset from Glasgow (resting state, eyes open). The analyzed signal length was 460 ± 32 s. For both datasets, we have performed Spectral Fingerprints analysis.

4. Results

Our first task was to check whether EEG SFs are similar to MEG SFs. To do this, we have visually examined spectral profiles in particular ROI (one-by-one), obtained from a different dataset and compared them (*e.g.* Fig. 1). SFs obtained both from MEG-O and from MEG-R were to a great extent coherent. However, the shapes of EEG SFs were not always similar. Extreme values for MEG SFs and EEG-A SFs were present more or less at the same frequencies, but in MEG SF, larger number of modes were present (Fig. 2). This is probably due to the fact that EEG technique does not resolve brain dynamics in higher frequencies as well as MEG [17] and thus information needed to find more spectral profiles is lost. Moreover, there is a discrepancy between fingerprints from different EEG datasets. These differences are at least partially explained by the lack of proper head models, requiring precise registration of sensor positions, as is evident from better results on smaller EEG-B dataset compared to EEG-A (*e.g.* Fig. 1). This issue will be carefully investigated in future research.

One of the most important goals of our study was to determine the specificity of spectral profiles for distinguishing individual brain areas using EEG data, which was never done before. We thus calculated the mean rank for each ROI (Fig. 3). A rank of 1 means the correct model area was the most likely to fit the test area; a rank of 2 means it was the second most likely, and so on. With random guess, rank value is $116/2 = 58$ (when the AAL atlas for parcellation of brain regions into 116 distinct ROIs is used [15] for the source analysis). Description of the calculation method can be found in [7] in the “Testing the Resting-State Models of Spectral Activity” section.

For the MEG-R data, we have obtained the mean rank of 2.4. Some errors in ranking are due to the difficulty of distinguishing fingerprints of left and right homologous regions. This result shows that spectral fingerprinting enables to untangle and separate activity of different brain regions. For the EEG datasets, the average rank was 10.0 for EEG-A data and 9.9 for the

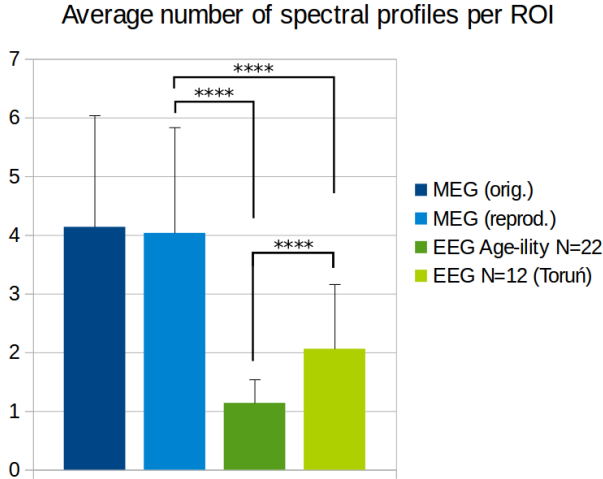


Fig. 2. Average number of spectral modes. Signal acquired using MEG has captured more distinct spectral profiles after using spectral fingerprinting than has been obtained from the EEG signal (EEG-A *vs.* MEG-R: Mann-Whitney $U = 19580$, $p < 10^{-4}$; EEG-B *vs.* MEG-R: Mann-Whitney $U = 17614$, $p < 10^{-4}$). Although EEG-B data includes 10 fewer subjects than EEG-A, it allowed for extraction of more spectral modes. Larger length of the signal and better registration of sensor positions is the most probable reason. The difference between MEG datasets in terms of the average number of spectral profiles is insignificant (Wilcoxon signed-rank test: $U = 1056.5$, $p = 0.16$). One-sided standard deviation bars were added. Negative parts of the error bars were neglected for clarity. Comparisons between EEG datasets with MEG-O dataset were omitted for clarity.

EEG-B data. Although it is well above the chance level, the results are not as good as in the case of MEG. This may be due to the fact that with the MEG technique, there is no volume conduction problem as when analyzing EEG, and thus source activity estimation is of much better quality, leading to more precise clustering of spectral patterns in the subsequent stages of Spectral Fingerprinting analysis.

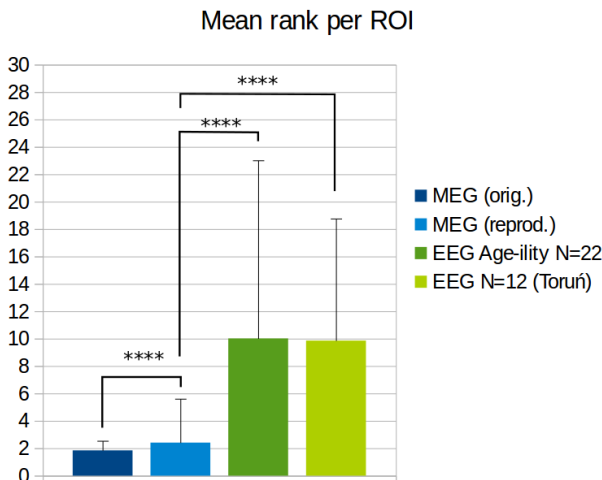


Fig. 3. Mean rank. There is a significant difference between EEG datasets and MEG datasets in terms of mean rank value: (Mann–Whitney: $U = 8194$, $p < 10^{-4}$) for MEG-R *vs.* EEG-A; (Mann–Whitney: $U = 7844.5$, $p < 10^{-4}$) for MEG-R *vs.* EEG-B. This means that building SFs using MEG entails more specific ROIs activity representations and thus easier classification of ROIs activity. The difference between EEG datasets in terms of the mean rank is insignificant (Mann–Whitney: $U = 13294$, $p = 0.67$). There was a significant difference between MEG datasets (Wilcoxon signed rank test: $U = 1667.5$, $p < 10^{-4}$). One-sided standard deviation bars were added. Negative parts of the error bars were neglected for clarity. Comparisons between EEG datasets with MEG-O dataset were omitted for clarity.

5. Conclusions and further studies of spectral fingerprints

Spectral fingerprinting is a procedure that allows for discovering spectral dynamics of each brain ROI from functional data (MEG, EEG). Each brain region has sufficiently specific fingerprint to classify it reliably when MEG recordings are available. For EEG, ROI recognition accuracy based on spectral fingerprints is not so precise although it still is quite useful. However, to be used in practical applications, further studies and improvements are needed. The EEG data used in this study had no information about precise position of electrodes, limiting the accuracy of the forward model. We plan to collect data from at least 22 subjects to have the same number of participants as in the Keitel and Gross study [7]. We will also check how placement of high-density EEG sensors effects the quality of the source reconstruction and spectral fingerprint ranking. A study by Liu *et al.* [22] shows that many small improvements lead to superior performance in terms of source activity estimation. We have recently developed a novel spatial filter approach for

solving inverse problems, called MV-PURE [23]. On simulated data, it resolves cortical dynamics better than well-known standard LCMV filter used by Keitel and Gross.

Obtaining high-quality spectral fingerprints should allow for investigation of brain states in the framework of dynamical system analysis. Transitions between different modes of brain activity, as manifested in several types of spectra at different times, seem to point at the attractor character of brain dynamics. Characterizing this non-linear dynamics will tell us a lot about processes in the brain. Ultimately, we are hoping that all these efforts will lead us to the better understanding of the human cognition and behavior. Mapping physical brain states into mental states that could be interpreted in subjective way may bridge the mind-body gap.

6. Tensor-based analysis of EEG signals

Our second example concerns perception of non-native phoneme contrasts in 8–12 months infants. In this period of development, the ability to discriminate non-native speech sounds is rapidly decreased [24]. Investigation of this phenomena is of great importance for understanding language acquisition in infancy. We have performed EEG experiments collecting the data that can shed light on this process. This is a very difficult task due to the technical problems of acquiring infant data, large number of artifacts in EEG, short speech stimuli, individual variation in baby development. There is a need for new ways of analyzing such data.

Mismatch Response (MMR) is a component of event-related potentials (ERPs) [25] elicited by a change in a repetitive acoustic pattern in an oddball experimental paradigm [26]. Experiments measuring ERPs are designed to reveal the specific perceptual and cognitive processes, analyzing various conventional features of ERPs including: peak measurements in the time-domain [25], the event-related oscillation in the frequency domain [27], the value derived from the region of interest in the time-frequency representation (TFR) [28] in the two domains, and also those features combined with the information in spatial domain to produce the topography of an ERPs [29, 30]. In this way, we are able to analyze the information in ERPs in one time window, frequency, time-frequency and spatial domains sequentially. It is beneficial to see analysis of the ERP experiments considering all of these features simultaneously [31], extracting features that may help to understand brain responses in a better way.

A multi-way data array (tensor) may represent all data of many participant's ERPs in time, frequency and the spatial domains. Decomposing such a tensor through a non-negative tensor factorization (NTF) method allows for extraction of multi-domain features from ERP recordings. Using multi-

domain features enables to perform analysis at the group level [31–33]. In other words, a multi-domain feature of an ERP can reveal the properties of the ERP in different domains simultaneously [31].

There are two basic models to perform non-negative tensor factorization, canonical polyadic decomposition (NCPD), also called parallel factor analysis (PARAFAC) [34, 35] and Tucker decomposition [36] under non-negativity constraints (NTD) [37]. The main difference between NCPD and NTD is that in the NCPD model, each extracted component in one mode is associated only with one extracted component in any other mode, while under the Tucker model, such a component can interact with any other component in any other mode. It is clear that the Tucker decomposition can provide much more possibilities to decompose a tensor than the NCPD model [38]. Cong *et al.* [39] have determined that the tensor decomposition for time-frequency representation of ERPs cannot be factorized with high accuracy through non-negative NCPD decomposition when the signal-to-noise ratio (SNR) in ERP data is low.

Given the N^{th} -order data tensor NCPD or NTD decompositions create N -component matrices in all modes and a core tensor. In the NCPD decomposition, the component matrix for subject mode is regarded as the multi-domain feature, while the core tensor in NTD is considered to carry the multi-domain feature. In the following, we are trying to answer two fundamental questions:

- how to choose relevant multi-domain features of an ERP among all extracted features for further analysis, and
- how to interpret selected multi-domain features based on the MMR experiments.

In this study, the tensor factorization is performed on the multi-way representation of MMRs elicited from experiments measuring EEG during passive oddball paradigm on native Polish infants. The passive oddball paradigm consisted of two types of deviant phonemes in syllables: 12.5% easy and 12.5% hard, and a standard presented in 75% of all cases.

7. Extracting multi-domain features of ERPs

Extracting a multi-domain feature for more reliable representation of the underlying source of brain activity to analyze processing of standard and deviant responses of infant’s brains in terms of the temporal, spectral, time-frequency representation (TFR) and spatial information simultaneously requires the following steps:

1. Data acquisition and preprocessing, removal of artifacts.
2. Segmentation of signal into time windows, time-frequency analysis.
3. Tensor generation.
4. Tensor factorization:
 - I. using NCPD approach;
 - II. using NTD approach;
 - III. finding the number of components;
 - IV. extracting the multi-domain feature.
5. Selection of interesting multi-domain features.

Data acquisition and preprocessing. EEG signals were recorded at 129 electrode sites using Geodesic Sensor Nets (Electrical Geodesics, Inc., Eugene, OR, USA) with the operating impedance below 50 K Ω . The sampling rate was 1000 Hz. The electrode COM, placed next to the central electrode (called Cz, using standard names from the extended 10/20 system for scalp electrode placement), was used to define a common ground. 14 electrodes giving most stable signal with lowest number of artifacts, placed mainly at the fronto-central area (Fz, F1, F2, F3, F4, FFC1h, FFC2h, FFC3h, FFC4h, FCz, FC1, FC2, CPz, Pz) were selected for further analysis. The data was down-sampled off-line to 128 Hz, band-passed filtered between 0.5–20 Hz and re-referenced to the mastoids (E57, E100), *i.e.* temporal bones behind the ears. Epochs time-locked to the stimulus onset were extracted. The length of the epoch was 900 ms, including a 100-ms pre-stimulus baseline. The artifact-contaminated epochs were automatically rejected if the amplitude of electrophysiological activity exceeded the absolute threshold of 120 μ V (usually due to muscle contraction and movements). The eye movements were removed using the ICA algorithm (runica, from EEGLab [29]). The remaining epochs were then visually inspected to check for other artifacts.

22 healthy native Polish infants (10 boys, mean age = 10 ± 1 month, age range 8–13 months) participated in the passive oddball paradigm experiments listening to the speech sounds. As shown in Fig. 4, this paradigm consists of two types of deviant syllables (12.5% easy and 12.5% hard) and a standard syllable (75%). Mismatch Response of infant’s brains to standard and deviant stimuli was recorded for all children.

Procedure

- *Oddball paradigm*: 2 types of deviant stimuli (15% „hard” and 15% „easy”) and standard (70%)

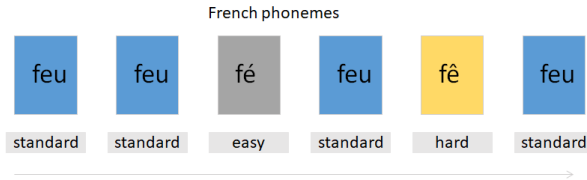


Fig. 4. Stimulus sequence.

In this experiment, three random variables are defined:

- The number of standard stimulus that should appear before one deviant is generated using geometric distribution with success probability $p = 1/3$, which implies that on average, there are 75% of standard stimuli and 25% of two kinds of deviant stimuli.
- A random variable for selection of “easy *vs.* hard deviant” is drawn from Bernoulli distribution with $p = 0.5$.
- A random variable drawn from exponential distribution with mean 100 ms is used for determining the length of jitter [40], varying the length of the interval between subsequent stimuli onsets.

Time-frequency analysis. For the time-frequency analysis of ERPs, fixed length sliding time window approach was used [41]. The time window has a fixed length independent of frequency. For each time window, the power is calculated. To avoid discontinuities that create spurious, high frequencies in the frequency analysis “tapering” of the recorded signal smoothly to zero at the start and end of the recording period is commonly used. We have used Hanning tapers (as available in MATLAB hann function). Please note that in the fixed window length procedure, the frequency resolution is defined according to the length of the time window. The frequency resolution in Hertz = $1/\text{length of time window in seconds}$. Since our whole trial interval is $[-0.1-0.79]$ s and our time of interest is $[0.5-0.7]$ s, we need to have at least a 0.2s window length. In this way, our time window enables only 5 Hz frequency resolution. The data analysis was performed using Fieldtrip toolbox [41].

Tensor generation. A fourth-order tensor \underline{Y} was constructed calculating TFR of all EEG channels. The tensor dimensions are based on frequency

× time × channel × subject. The number of frequency bins (I_f), timestamps (I_t), channels (I_c), and subjects (I_s) defines the dimension of the whole tensor $\underline{Y} \in R_+^{I_f \times I_t \times I_c \times I_s}$.

Tensor factorization. Two methods of factorization may be used, but here, only the simpler NCPD model is introduced for finding the number of relevant components and choosing interesting multi-domain features from all extracted components.

Non-negative canonical polyadic decomposition (NCPD). The NCPD model can be formulated as follows [37]. For a given N^{th} -order tensor $\underline{Y} \in R_+^{I_1 \times I_2 \times \dots \times I_N}$, perform a factorization into N unknown non-negative matrices whose elements are non-negative: $U^{(n)} = [u_1^{(n)}, u_2^{(n)}, \dots, u_J^{(n)}] \in R_+^{I_n \times J}$, $n = 1, 2, \dots, N$, represent common factors that can be used to recreate original tensor

$$\underline{Y} \approx \sum_{j=1}^J u_j^{(1)} \circ u_j^{(2)} \circ \dots \circ u_j^{(N)}, \quad (1)$$

where $\|u_j^{(n)}\|_2 = 1$, for $n = 1, 2, \dots, N - 1, j = 1, 2, \dots, J$, and the symbol ‘ \circ ’ denotes the outer product of vectors. The target of NCPD algorithm is to obtain suitable matrices $U^{(n)}$. Different J here correspond to different approximations of the NCPD model. The NCPD decomposition can also be written in the tensor product form

$$\underline{Y} \approx \underline{I} \times_1 U^{(1)} \times_2 U^{(2)} \dots \times_N U^{(N)} = \widehat{\underline{Y}}, \quad (2)$$

where $\widehat{\underline{Y}}$ is an approximation of the tensor \underline{Y} and \underline{I} is the identity tensor. Each factor $U^{(n)}$ contributes to the whole tensor along the corresponding data mode. Most algorithms for NCPD minimize the squared Euclidean distance (Frobenius norm) given by the following cost function:

$$D(\underline{Y} | \widehat{\underline{Y}}) = \frac{1}{2} \left\| \underline{Y} - \underline{I} \times_1 U^{(1)} \times_2 U^{(2)} \dots \times_N U^{(N)} \right\|_F^2. \quad (3)$$

Finding the number of components. Determining the number of extracted components in each factor in both NCPD and NTD decompositions is a crucial issue [37], because different numbers of factors may correspond to quite different decomposition results. Only the components that cover most important aspects of the data should be created. Here, we have used difference of fits method (DIFFIT) [42] for estimating the number of components to be extracted using the NCPD model. This method was originally

developed for the three-mode principal components analysis, but can be extended to higher-order tensor decompositions. The number of components is invariable across different factors, so just one parameter should be determined by DIFFIT method. The definition of DIFFIT is introduced as follows. The fit of a NTF model is defined as

$$\text{fit}(m) = 1 - \frac{\|\underline{Y} - \widehat{\underline{Y}}_m\|_F}{\|\underline{Y}\|_F},$$

where $\widehat{\underline{Y}}_m$ is the approximation to raw data tensor \underline{Y} in the m^{th} model of tensor factorization using the certain number of extracted components $m = 1, 2, \dots, M$. Then the difference fit of the two adjacent fits is

$$\text{dif}(m) = \text{fit}(m) - \text{fit}(m - 1),$$

where $m = 2, 3, \dots, M$. Next, the ratio of the adjacent difference fits reads as

$$\text{diffit}(m) = \frac{\text{dif}(m)}{\text{dif}(m + 1)},$$

where $m = 2, 3, \dots, M - 1$. The model with the largest diffit value is considered to be the optimal for the factorization of original data tensor \underline{Y} .

Extracting the multi-domain feature. After decomposition of the fourth-order tensor \underline{Y} , components include modes of the frequency, time, channel and subjects. Now, it is important to recognize which component matrix in factorized tensor can carry important multi-domain features. In NCPD, decomposed tensor contains J components in each mode

$$\underline{Y} \approx \sum_{j=1}^J u_j^{(f)} \circ u_j^{(t)} \circ u_j^{(c)} \circ f_j = \underline{I} \times_1 U^{(f)} \times_2 U^{(t)} \times_3 U^{(c)} \times_4 F. \quad (4)$$

The component matrix for the subject mode F contains the multi-domain features, extracted brain responses represented by combinations of factors in the subspaces spanned by the spectral ($U^{(f)}$), temporal ($U^{(t)}$) and spatial ($U^{(c)}$) factors.

Selecting the desired multi-domain features. After extraction of a number of components selection, the process to find most informative multi-domain feature is done. A fourth-order tensors \underline{Y} with dimensions of frequency (4 frequency bins), time (26 time frames), channel (14 electrodes) and subjects (44) are created, using two types of stimuli, EEG recordings from interval [0.5 0.7] s. Here, subject dimension is 44 because we take standard and easy stimulus separately, each with 22 subjects, and then hard and standard separately. The first 22 positions represent standard stimulus over all 22 subjects, and the remaining ones, one of the deviants.

8. Tensor decomposition results

Results of the NCPD factorization are present here in two ways. First, decomposition for standard stimulus and easy deviant for all subjects is analyzed to remove components that carry little information. We have also rearranged the order of the subject component placing at the first positions data for 11 younger infants (8 to 9 months) and the remaining data for older infants as the next 11 subjects. We did not run the tensor decomposition again, just rearranged the subject component of the current tensor decomposition in a way that infants are separated based on their age and keeping only the noise-free components. The selection of such components is based on the variance of the signal in at least one of the domains (time, space, frequency); if this variance is very small, there is no information in the component and it may be removed.

For each obtained decomposition, we need to display and analyze the results, choose the free-of-noise components, and try to interpret the results. As the whole, analysis take a lot of space, only examples are presented here, using single selected feature and a few subjects.

Multi-domain features of tensor by NCPD: Standard-easy

- DIFFIT method suggested that 27 components were appropriate for NCPD. The feature #13 was chosen as the most informative multi-domain feature among all 27 extracted features. The results is shown in Fig. 5.
- Strong right-side asymmetry is present in the low-frequency theta (top right corner). This may indicate that there is right-hemispheric advantage in theta rhythm representing anticipation of incoming stimuli, a dynamical process of expectancy and surprise corresponding to detection of deviant as reflected in the MMR.
- After removing components that contain mostly noise, we are left with features [7, 9, 10, 11, 12, 13, 15, 18]. In Fig. 5, one can see feature #14 that is an example of such a noise component.

Standard-easy case with age separation

In Fig. 6, subject component is rearranged to show younger infants (8 to 9 months) first, for the standard and easy stimulus, with older infants on the right-hand side. The spatial component is represented by the magnitude for selected electrodes. Only the noise-free components are shown.

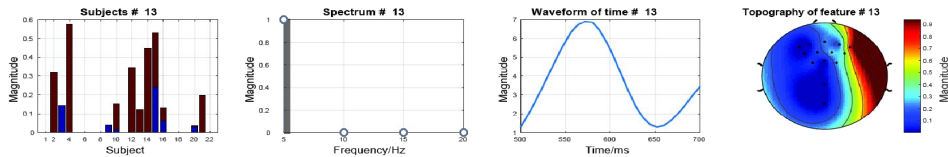


Fig. 5. (Color online) Factor extracted by NCPD. In subject plot (left column), the gray/blue bar and black/brown bar indicate the standard stimuli and easy deviant respectively. Second column shows the spectral bin of 5 Hz width, third, the temporal change of the waveform for this component, and the right column shows spatial component.

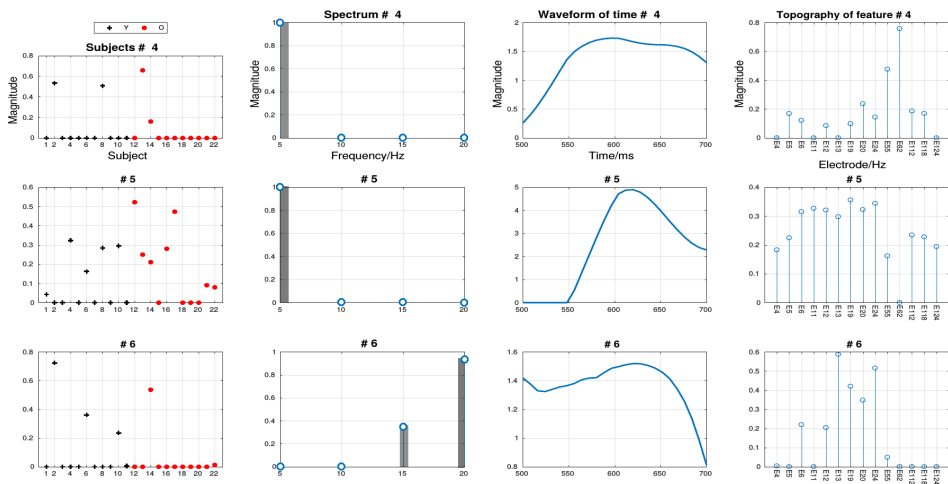


Fig. 6. Example of three factors extracted by NCPD. In the subject plot, the order of infants are rearranged based on their ages.

9. Future research steps for tensor decomposition

The infant data is quite noisy, with many artifacts and very short time window in which mismatch response is expected, therefore, very difficult to analyze. Such an analysis should extract multidimensional information that experts will be able to interpret about infant's brains processes responsible for speech perception and reactions to phonemic contrasts.

We have presented here the most difficult case, contrasting standard and easy deviant stimuli. The focus on the interval where MMR is expected is justified by literature [26] but perhaps longer-time windows will allow for better frequency resolution without losing the mismatch reaction.

Still tensor decomposition is able to find interesting components that can be interpreted by experts. The process may be repeated generating tensors for the pair of easy deviant *vs.* hard deviant, and standard deviant *vs.* hard

deviant. An alternative is to generate three tensors, each based on just one stimulus (Standard–Easy–Hard) and noise-free components. Decomposed results will be arranged according to the age of infants, and components from tensor decomposition interpreted by experts.

10. Summary

In the first paper [43], a sketch of a long road towards understanding of brain dynamics has been presented, stressing the importance of the network level. Global brain initiatives should lead to collaboration of experts from many branches of science at a large scale. The level at which brain is described depends on questions that are being asked. Research Domain Criteria (RDoC) introduced as classification framework for research on mental disorders is based on multi-level neuropsychiatric phenomics [44], including genetic, molecular, cellular, circuit, physiological systems, behavior and subjective self reports level. To understand reactions of the brain to drugs, one need to work on the molecular and cellular level. To understand subjective experiences at the mental level, psychological constructs are used.

In our research, we are focused on the middle, neural circuit level. Computational models help to understand how lower levels influence large-scale neurodynamics and lead to hypothesis that should be verified experimentally. We have shown this in the case of autism and ADHD. Verification requires experiments and analysis of brain signals. In the second paper on multi-level explanations in neuroscience, we have shown how real EEG/MEG brain signals may be analyzed to discover brain activity in selected regions of interest. The EEG Spectral Fingerprint approach will be tested on resting state data that are being collected with proper registration of EEG electrode positions. Such a registration requires either specialized equipment based on electromagnetic or ultrasound digitization, geodesic photogrammetry, or images obtained in MRI scanner with the EEG cap on the head. Such approaches have not yet been used to analyze infant EEG data related to development of speech perception. Tensor decomposition of event-related potentials may help in this case to interpret some processes.

Ultimately computational modeling and real brain signal analysis methods should help to create models of neurodynamics that explain animal and human development and behavior.

This study was partially supported by the National Science Centre, Poland (NCN), grant No. UMO-2016/20/W/NZ4/00354 (mainly data acquisition), and grant No. UMO-2013/08/W/HS6/00333 (mainly data analysis), awarded to our group. We also gratefully acknowledge support from authors of the spectral fingerprint publication, Dr. Anne Keitel and Prof. Joachim Gross from the University of Glasgow.

REFERENCES

- [1] W. Duch, *Comput. Phys. Commun.* **97**, 136 (1996).
- [2] G. Caldarelli, S. Wolf, Y. Moreno, *Nature Phys.* **14**, 870 (2018).
- [3] J.S. Damoiseaux *et al.*, *Cereb. Cortex* **18**, 1856 (2008).
- [4] M. Rosanova *et al.*, *J. Neurosci.* **29**, 7679 (2009).
- [5] F.M. Krienen, B.T.T. Yeo, R.L. Buckner, *Phil. Trans. R. Soc. B* **369**, 20130526 (2014).
- [6] W. Singer, *Trends Cogn. Sci.* **17**, 616 (2013).
- [7] A. Keitel, J. Gross, *PLoS Biol.* **14**, e1002498 (2016).
- [8] R.D. Pascual-Marqui, *Int. J. Bioelectromagn.* **1**, 75 (1999).
- [9] P. Ramkumar, L. Parkkonen, A. Hyvärinen, *NeuroImage* **86**, 480 (2014).
- [10] A. Hillebrand *et al.*, *NeuroImage* **59**, 3909 (2012).
- [11] A. Puce, M.S. Hämäläinen, *Brain Sci.* **7**, 58 (2017).
- [12] W.O. Tatum, *Handbook of EEG Interpretation*, Demos Medical Pub. New York, 2013.
- [13] R.A. Poldrack, J.A. Mumford, T.E. Nichols, *Handbook of Functional MRI Data Analysis*, Cambridge University Press, 2011.
- [14] S. Baillet, J.C. Mosher, R.M. Leahy, *IEEE Signal Processing Mag.* **18**, 14 (2001).
- [15] N. Tzourio-Mazoyer *et al.*, *NeuroImage* **15**, 273 (2002).
- [16] F. Karayanidis *et al.*, *NeuroImage* **124**, 1137 (2016).
- [17] M.X. Cohen, *Analyzing Neural Time Series Data: Theory and Practice*, MIT Press, 2014.
- [18] J.G. Proakis, D.K. Manolakis, *Digital Signal Processing*, 4th ed., Pearson, Upper Saddle River, N.J. 2006.
- [19] B.D. Van Veen, W. Van Drongelen, M. Yuchtman, A. Suzuki, *IEEE Trans. Biomed. Eng.* **44**, 867 (1997).
- [20] J. Gross *et al.*, *Proc. Natl. Acad. Sci. USA* **98**, 694 (2001).
- [21] M.S. Hämäläinen, R.J. Ilmoniemi, *Med. Biol. Eng. Comput.* **32**, 35 (1994).
- [22] Q. Liu, M. Ganzetti, N. Wenderoth, D. Mantini, *Front. Neuroinform.* **12**, 4 (2018).
- [23] T. Piotrowski, J. Nikadon, D. Gutierrez, [arXiv:1712.02997](https://arxiv.org/abs/1712.02997) [eess.SP].
- [24] M. Saxton, *Child Language: Acquisition and Development*, SAGE Publications Ltd., Los Angeles 2010.
- [25] S.J. Luck, *An Introduction to the Event-related Potential Technique*, MIT Press, Cambridge, MA, 2005.
- [26] R. Näätänen, A.W.K. Gaillard, S. Mäntysalo, *Acta Psychol.* **42**, 313 (1978).
- [27] G.G. Yener, E. Başar, *Cogn. Neurodyn.* **4**, 263 (2010).
- [28] G. Stefanics *et al.*, *Psychophysiology* **44**, 697 (2007).
- [29] A. Delorme, S. Makeig, *J. Neurosci. Methods* **134**, 9 (2004).

- [30] L. Fuentemilla, J. Marco-Pallarés, T.F. Münte, C. Grau, *Brain Res.* **1220**, 93 (2008).
- [31] F. Cong *et al.*, *Int. J. Neural Syst.* **22**, 1250025 (2012).
- [32] F. Cong *et al.*, *Lect. Notes Comput. Sci.* **7191**, 502 (2012).
- [33] F. Cong *et al.*, *Lect. Notes Comput. Sci.* **6365**, 620 (2010).
- [34] F.L. Hitchcock, *J. Math. Phys.* **6**, 164 (1927).
- [35] R.A. Harshman, *UCLA Working Papers in Phonetics* **16**, 1 (1970).
- [36] L.R. Tucker, *Psychometrika* **31**, 279 (1966).
- [37] A. Cichocki, R. Zdunek, A.H. Phan, S-i Amari, *Nonnegative Matrix and Tensor Factorizations: Applications to Exploratory Multi-way Data Analysis and Blind Source Separation*, John Wiley and Sons, 2009.
- [38] E. Acar, Y. Bülent, *IEEE Trans. Knowledge Data Eng.* **21**, 6 (2009).
- [39] F. Cong *et al.*, *Int. J. Neural Syst.* **23**, 1350006 (2013).
- [40] R. Stephens, *The Meaning of Total Jitter*, Tektronix publication, 2007.
- [41] R. Oostenveld, P. Fries, E. Maris, J.M. Schoffelen, *Comput. Intell. Neurosci.* **2011**, 156869 (2011).
- [42] M.E. Timmerman, H.A.L Kiers, *Br. J. Math. Stat. Psychol.* **53**, 1 (2000).
- [43] W. Duch, *Acta Phys. Pol. B* **49**, 9999 (2018), this issue.
- [44] T. Insel *et al.*, *Am. J. Psychiat.* **167**, 748 (2010).